

Mechanisms for the Extraction of Tropopause Polar Vortices and Associated Surface-based Pools of Arctic Air from High Latitudes and their Transport to Middle Latitudes

Kevin A. Biernat

ATM 619: Cyclone Workshop Seminar
Spring 2016

*Department of Atmospheric and Environmental Sciences, University at Albany,
State University of New York, Albany, New York*

ABSTRACT

Coherent vortices in the vicinity of the tropopause, referred to as tropopause polar vortices (TPVs), may be extracted from high latitudes in conjunction with high-latitude upper-level ridge amplification events. Once extracted, TPVs may interact with and strengthen midlatitude jet streams, as well as act as precursor disturbances for intense midlatitude cyclogenesis events and extreme weather events. Surges of arctic air also may accompany TPVs as they are transported to middle latitudes and may lead to widespread cold air outbreaks (CAOs). This study will explore the 1) the mechanisms responsible for the extraction of TPVs from high latitudes and their transport to middle latitudes and 2) the relationship between these TPVs and cold surges through two multiscale case study analyses. The case studies selected are 1) the 9–11 January 1982 CAO over central and eastern North America and 2) the 13–14 February 2016 CAO over eastern North America.

Preceding the equatorward transport of the TPVs in each case is upstream ridge amplification over the eastern North Pacific and western North America. The TPVs are transported equatorward within the northerly flow downstream of these ridges. Beneath each TPV is a pool anomalously cold, arctic air. Meridional cross sections transecting each TPV and associated pool of arctic air indicate the presence of an arctic front and tropopause folding extending downward and equatorward from each TPV. The interaction of the strong January 1982 TPV with a strong northerly flow jet on the downstream side of the upstream ridge leads to quasi-geostrophic (QG) forcing for descent and concomitant rapid strengthening of a surface anticyclone to 1062 hPa, as well as forcing for upper-level frontogenesis. In each case, strong cold air advection between a strong upstream surface anticyclone and downstream surface cyclone allows the arctic air beneath and behind the TPV to be transported equatorward.

1. Introduction

Thorpe (1985) and Hoskins et al. (1985) were among of the first to conceptualize tropopause vortices from a potential vorticity (PV) perspective as upper-level, cyclonic PV anomalies. These cyclonic PV anomalies feature a downward depression in the height of the dynamic tropopause (DT), with anomalously cold (warm) air found below (above) the depressed tropopause. Hakim and Canavan (2005) and Cavallo and Hakim (2009) formally introduced the term “TPV.” For their purposes, they defined TPVs as coherent, tropopause-based vortices that spend at least 60% of their lifetime north of 65°N and last at least 2 days. A TPV is a particular type of coherent tropopause disturbance (CTD; Pyle et al. 2004; Kravitz 2007), which is a tropopause-based material feature that is not necessarily of high-latitude origin.

Past studies have shown that ridge amplification may lead to the extraction of TPVs/CTDs from the high latitudes and their transport to middle latitudes. Hakim et al. (1995, 1996) illustrated that a CTD contributing to the development of the 1978 Cleveland Superbomb was transported from the Arctic to the Ohio Valley downstream of a ridge over the eastern North Pacific and western North America. Bosart et al. (1996) showed that northwesterly flow downstream of an amplifying ridge transported a long-lived arctic CTD into the middle latitudes that contributed to the development of the Superstorm of 1993. Based on these studies, it is hypothesized that the northerly flow found just downstream of amplifying ridges supports the extraction of TPVs from high latitudes and their transport to middle latitudes. Disturbances such as extratropical cyclones (ETCs) may play important roles in leading to these amplifying ridges.

Shapiro et al. (1987) illustrated a possible connection between the equatorward migration of high-latitude disturbances and CAOs over the middle latitudes. Shapiro et al. (1987) showed that the equatorward migration of a “polar vortex” downstream of a ridge over western North

America during January 1985 was associated with a CAO over central and eastern North America. Arctic air was found beneath the vortex and behind an arctic front associated with the vortex that swept quickly across eastern North America as the vortex migrated southeastward, resulting in daily minimum temperature records from the Great Lakes to southern Florida. Figure 1 shows a plot of the 500-hPa geopotential height field at 0000 UTC 20 January 1985 [adapted from Fig. 5 in Shapiro et al. (1987)], along with a corresponding plot of the DT potential temperature and wind fields obtained from the 0.5° National Centers for Environmental Prediction (NCEP) Climate Forecast System Reanalysis (CFSR) global gridded dataset (Saha et al. 2010, 2014). Figure 1 indicates that coincident with the “polar vortex” at 500 hPa is a strong TPV characterized by minimum potential temperature on the DT of 260–264 K. Based on this study, it is hypothesized that TPVs can serve as catalysts for CAOs as the arctic air found beneath and behind TPVs surges equatorward as TPVs are transported into middle latitudes.

A commonality associated with CAOs over North America is surface anticyclogenesis over northwestern North America prior to CAO onset (Colucci and Davenport 1987). In a composite of Alaskan strong anticyclones, Jones and Cohen (2011) showed that there is strong QG forcing for subsidence associated with the strong vertical circulation in the composite jet entrance region over the strengthening anticyclone located downstream of a ridge. Given that the equatorward transport of TPVs may occur along with cold surges raises the question of whether TPVs play a role in the formation and/or strengthening of surface anticyclones characteristic of CAOs. For example, Pyle et al. (2004) indicated that the close approach of a TPV with a northerly flow jet streak located on the downstream side of a ridge over western North America led to the strengthening of this jet streak. It is hypothesized that the strengthening of jet streaks due to TPV–jet interaction, may lead to stronger secondary ageostrophic circulations associated

with stronger subsidence, which may support the development of stronger surface anticyclones that promote more intense cold surges.

In order to address these forgoing hypotheses, multiscale case study investigations of two TPVs associated with CAOs are presented. The cases selected for investigation are 1) the 9–11 January 1982 CAO over central and eastern North America and 2) the 13–14 February 2016 CAO over eastern North America. Both CAOs occurred as a TPV was transported to middle latitudes and both resulted in minimum temperature records across portions of North America.

2. Data and Methodology

The multi-scale case study investigations of the two TPVs and associated CAOs are conducted utilizing the 0.5° NCEP CFSR dataset. TPVs are tracked subjectively by following the minimum of DT potential temperature associated with each TPV from genesis (first occurrence of closed DT potential temperature contours) to lysis (when the TPV became substantially deformed through interaction with the North Atlantic jet stream). The QG forcing for vertical motion as the TPV approaches and/or interacts with the northerly flow jet streak located on the downstream side of the upstream ridge in each case is examined. The Q vector is calculated in pressure coordinates using the following equation from Hoskins and Pedder (1980):

$$\mathbf{Q} = -\left(\frac{\partial \mathbf{V}_g}{\partial x} \cdot \nabla_p \theta\right) \mathbf{i} - \left(\frac{\partial \mathbf{V}_g}{\partial y} \cdot \nabla_p \theta\right) \mathbf{j}, \quad (1)$$

where \mathbf{V}_g is the geostrophic wind, θ is the potential temperature, and ∇_p is the horizontal gradient operator along a constant pressure surface. Q-vectors are separated into their along-isentrope (\mathbf{Q}_s) and across-isentrope (\mathbf{Q}_n) components following Keyser et al. (1992) as follows:

$$\mathbf{Q}_s = \left(\frac{\mathbf{Q} \cdot (\mathbf{k} \times \nabla \theta)}{|\nabla \theta|}\right) \frac{\mathbf{k} \times \nabla \theta}{|\nabla \theta|} \quad (2)$$

$$\mathbf{Q}_n = \left[\mathbf{Q} \cdot \left(-\frac{\nabla\theta}{|\nabla\theta|} \right) \right] \left(-\frac{\nabla\theta}{|\nabla\theta|} \right). \quad (3)$$

Q vector forcing for vertical motion associated with \mathbf{Q}_s and \mathbf{Q}_n are calculated using the Q vector form of the omega equation in pressure coordinates from Hoskins and Pedder (1988), given by

$$\left(\sigma \nabla_p^2 + f_0^2 \frac{\partial^2}{\partial p^2} \right) \omega = -2h(\nabla_p \cdot \mathbf{Q}), \quad (4)$$

with \mathbf{Q} replaced by \mathbf{Q}_s and \mathbf{Q}_n , respectively. $h = (\rho \theta)^{-1}$, or equivalently, $h = \frac{R}{p_0} \left(\frac{p_0}{p} \right)^{c_v/c_p}$, f_0 is a constant reference value of the Coriolis parameter, R is the dry gas constant, p is the pressure, p_0 is 1000 hPa, ∇_p is the horizontal gradient operator along a constant pressure surface, c_v is the specific heat of dry air at constant volume, and c_p is the specific heat of dry air at constant pressure, σ is the stability parameter and ω is the vertical pressure velocity. These Q vector components and their associated forcings for vertical motion are calculated every 100 hPa for the 600–400-hPa layer and then averaged. The 600–400-hPa layer was chosen as it represents the layer in which a large proportion of the TPV is located in each case. \mathbf{Q}_s (\mathbf{Q}_n) describe the rate of change of the direction (magnitude) of $\nabla\theta$ (Keyser et al. 1992).

3. TPV Tracks

The track maps for these TPVs are shown in Fig. 2. Figure 2 also shows the time-mean 300-hPa geopotential heights and standardized anomalies for the time period during which the TPV in each case is transported equatorward into middle latitudes. The January 1982 TPV was long-lived, lasting approximately 31 days (Fig. 2a). After spending most of its lifetime meandering over northern Canada, it quickly moved equatorward ahead of an anomalous ridge located over the eastern North Pacific and western North America (Fig. 2a). The February 2016 TPV has a shorter lifetime (~8 days), as it was quickly transported equatorward ahead of an

anomalous ridge located over the Arctic after genesis and later ahead of an anomalous ridge located over western North America (Fig. 2b). In both cases, an anomalous long-wave trough is noted over eastern North America. The northerly flow between the anomalous upstream ridge and downstream trough in each case appears to be important in the equatorward transport of these TPVs to middle latitudes. The mechanisms responsible for the development and amplification of these ridges will be investigated in the next section.

4. TPV Extraction

a. January 1982 case

The mechanisms responsible for the development of anomalous ridging over western North America during the extraction of the January 1982 TPV are first investigated. At 0000 UTC 6 January 1982, an amplifying ridge is located over the eastern North Pacific just downstream of a trough (Fig. 3a) associated with multiple vorticity maxima (not shown). An occluded ETC that previously underwent explosive deepening is located upstream of the ridge, along with an amplifying secondary ETC just to the south of the occluded ETC (Fig. 3b). A plume or relatively high precipitable water (PW) values exceeding 25 mm associated with an implied warm conveyor belt (WCB) is found just downstream of the ETCs. Lower-tropospheric warm air advection within the WCB, indicated by the nearly perpendicular orientation of the mean sea level pressure (MSLP) gradient to the 1000–500-hPa thickness gradient (Fig. 3b) contributes to the aforementioned ridge amplification. Furthermore, upper-tropospheric divergent outflow emanating from regions of ascent in the vicinity of the ETC and WCB leads to upper-tropospheric negative PV advection by the irrotational wind, further contributing to the aforementioned ridge amplification as well (not shown).

By 1200 UTC 7 January the ridge has continued to amplify downstream of the narrowing upstream trough (Fig. 3c). A narrow corridor of relatively high PW air exceeding 25 mm extends from the subtropics to just south of the Gulf of Alaska downstream of the aforementioned secondary ETC within the WCB (Fig. 3d). Lower-tropospheric warm air advection has intensified just offshore western Canada as the gradients of MSLP (1000–500-hPa thickness) have strengthened between the ETC (thermal ridge) over the eastern North Pacific and strong surface anticyclone (surface-based pool of arctic air) over northwestern Canada (Fig. 3d). This lower tropospheric warm air advection along with negative PV advection by the irrotational wind (not shown) has continued to support the amplification of the ridge.

By 0000 UTC 9 January, the ridge has continued to amplify and move eastward into western North America, coming into closer proximity with the TPV (Fig. 3e). The strong thermal gradient between the ridge and TPV/associated surface-based pool of arctic air has resulted in the intensification of a strong northerly flow jet streak to over 100 m s^{-1} over southwestern Canada (Figs. 3e,f). The northerly flow on the downstream side of the ridge contribute to the equatorward transport of the TPV into the United States, as will be shown in Section 5.

b. February 2016 case

Figure 4a shows that at 0000 UTC 7 February 2016, the TPV of interest is located over the high Arctic, to the east of a region of broad anticyclonic flow located just north of eastern Russia. This region of anticyclonic flow, characterized by positive 300-hPa geopotential height standardized anomalies of $+1.5$ to $+3\sigma$, has been a persistent feature since late January 2016 (not shown). Repeat episodes of rapidly deepening ETCs over the north Pacific in the left exit region of a strong, zonal Pacific jet from late January into early February have lead to repeat poleward

transports of low PV air into high latitudes during this time frame, likely contributing to the maintenance of the anticyclone over the Arctic (not shown). Further to the south at 0000 UTC 7 February, an occluded ETC that has previously undergone explosive cyclogenesis is located near the Gulf of Alaska (Fig. 4b). Lower tropospheric warm air advection downstream of the ETC within the WCB (Fig. 4b) has likely contributed to the development and amplification of the ridge over the eastern North Pacific and western North America seen in Fig. 4a. Furthermore, upper-tropospheric irrotational outflow extending from regions of ascent in the vicinity of the ETC and WCB has led to upper-tropospheric negative PV advection by the irrotational wind, further contributing to the aforementioned ridge amplification (not shown).

By 0000 UTC 9 February, the TPV has moved equatorward within the northerly flow downstream of the anticyclone over the Arctic (Fig. 4c). A short-wave trough in the exit region of the strong North Pacific jet (Fig. 4c) has led to the development of another ETC just downstream (Fig. 4d). Lower-tropospheric warm air advection along with upper-tropospheric negative PV advection by the irrotational wind downstream of this ETC have contributed to the maintenance and amplification of the downstream ridge over western North America during the past 48 hours (not shown).

By 0000 UTC 11 February, the TPV has continued to move equatorward and is now located within the northerly flow on the downstream side of the ridge over western North America (Fig. 4e). This northerly flow will allow the TPV to continue moving equatorward over central and eastern North America. Broad cyclonic flow in the eastern North Pacific in the exit region of the North Pacific jet (Fig. 4f) promotes continued downstream southerly flow and lower-tropospheric warm air advection, leading to ridge maintenance over western North America.

5. Relationship between TPVs and CAOs

a. January 1982 case

From 8 to 10 January 1982, the TPV of interest is transported into the middle latitudes, concurrent with the occurrence of a CAO over central and eastern North America. At 1200 UTC 8 Jan 1982, the strong TPV associated with minimum DT potential temperature values between 252 and 255 K (Fig. 5a) is coincident with a 1000–500-hPa thickness minimum of less than 470 dam (Fig. 5b). Between the upstream ridge and the TPV is a strong, 1048-hPa surface anticyclone located in the left entrance region of the strong northerly flow jet (Figs. 5a and 5b). The TPV becomes juxtaposed with the upstream ridge by 1200 UTC 9 January (Fig. 5c) as it moves southeastward along with the pool of arctic air (Fig. 5d). The surface anticyclone over northwestern North America has expanded eastward and strengthened (Fig. 5d) to 1056-hPa (not shown) in the left entrance region of the jet. 24 hours later, the TPV and associated pool of arctic air have moved southeastward into the base of the longwave trough over eastern North America (Fig. 5e). The upstream surface anticyclone has continued to intensify over the past 24 hours, and has rapidly expanded southeastward over the Great Plains, with strong cold air advection evident over much the south-central and southeastern portions of the United States, given the nearly perpendicular orientation of the strong SLP gradient to the 1000–500-hPa thickness gradient in these areas (Fig. 4f). The SLP gradient is likely enhanced due to the presence of strong surface ETCs downstream over James Bay and just south of Labrador.

Figure 6 shows a meridional cross section transecting the TPV and associated pool of arctic air at 1800 UTC 9 January. At this time, the TPV is juxtaposed with the upstream ridge. Figure 5 shows essentially a deep PV wall separating the ridge (characterized by PV values generally <0.5 PVU) from the strong TPV (characterized by PV values >2 PVU) extending

downward to approximately 850 hPa. Strong, tropospheric-deep baroclinicity, between the ridge and TPV supports the strong northerly flow jet streak with winds exceeding 80 m s^{-1} within the jet core. Beneath the TPV, isentropes bend upward, indicative of the pool of arctic air found beneath the TPV evidenced in Figs. 5b,d,f by the collocation of the TPV with the 1000–500-hPa thickness minimum. The presence of a pool of arctic air beneath the TPV is unsurprising as the composite cross-section of TPVs by Cavallo and Hakim (2010) has shown that a core of anomalously cold air is found directly beneath the composite TPV.

An arctic front is evidenced by the sloping region of relatively high PV air and large vertical gradient of potential temperature extending downward and equatorward from the TPV. The sloping nature of the 2 PVU surface within the upper portion of the arctic front indicates tropopause folding beneath the jet. The leading edge of the Arctic front can be seen near the surface, south of 40°N , where there is a relatively large horizontal gradient of potential temperature near the surface. Beneath the arctic front within the boundary layer, a mixed layer is apparent and the air appears to be unstable given $-\frac{\partial\theta}{\partial p} \leq 0$. A similar result is shown by Shapiro et al. (1987) with cross sections transecting the “polar vortex” and associated arctic front from January 1985 (their Figs. 9 and 10). They suggested that this unstable air results from diabatic heating induced by the flow of arctic air over the relatively warm land surface. Figure 6 also indicates a shallow band of relatively high PV air characterized by a strong vertical gradient of potential temperature extending poleward and downward toward the surface from the TPV. The strong vertical potential temperature gradient near the surface indicates a steep temperature inversion, the development of which is likely tied to strong longwave radiative cooling that typically occurs over the high latitudes during the Boreal Winter (Emanuel 2008).

The strengthening of the surface anticyclone in the left entrance region of the northerly flow jet as the TPV closely approaches this jet (Fig. 5) brings into question the role of the TPV in the strengthening of this anticyclone. Figure 7 shows plots of 600–400-hPa Q_n and Q_s and their respective forcings for vertical motion from 0600 UTC to 1800 UTC 9 January 1982, the time frame during which the TPV closely approaches and interacts with the northerly flow jet and during which the surface anticyclone exhibits its greatest intensification. At 0000 UTC 9 January 1982, Q_n forcing for descent occurs slightly south and east of the core of the 1050-hPa anticyclone located over northwestern Canada (Fig. 7a). The orientation of the Q_n vectors from warm to cold air suggest that upper-level frontogenesis is potentially occurring and that the direct ageostrophic thermal circulation in the entrance region of the jet may be strengthening as the magnitude of the thermal gradient strengthens due to the TPV–jet interaction. Fig. 7b also shows that Q_s forcing for descent occurs just south and east of the surface anticyclone core as well. Furthermore, geostrophic cold air advection is evident in the region of Q_n and Q_s forcing for descent, noted by the relatively large angle between the geopotential height gradient and the potential temperature gradient (Figs. 7a,b). This cold air advection is maximized on the cyclonic shear side of the northwesterly flow jet (not shown). Shapiro (1981) has shown that cold air advection in cyclonic shear provides a favorable environment for upper-level frontogenesis, which is suggested by the orientation of the Q_n vectors as described previously.

The forcing for descent by Q_s and Q_n to the southeast of the core of the surface anticyclone at 0600 UTC 9 January suggests that the anticyclone will build southeastward and potentially intensify. Indeed, by 1200 UTC 9 January, the surface anticyclone has rapidly strengthened by 6 hPa from 1050 to 1056 hPa while moving southeastward to northern Saskatchewan. Continued Q_n (Fig. 7c) and Q_s (Fig. 7d) forcing for descent continues to occur

just southeast of the surface anticyclone, suggesting a continued southeastward expansion and potential intensification of the surface anticyclone. This indeed occurs, as the surface anticyclone moves slightly southeastward and intensifies by 4 hPa to 1060-hPa. Furthermore, both Q_n and Q_s forcing for descent (Figs. 7e and 7f, respectively) have both increased slightly southeast of the core of the anticyclone. The anticyclone will go on to intensify another 2 hPa to 1062 hPa by 0000 UTC 10 January. Figs. 7c–f also indicate continued geostrophic cold air advection in the regions of Q_n and Q_s forcing for descent, suggesting continued upper-level frontogenesis, which is also evident by the Q_n vectors continuing to be directed toward warm air in Figs. 7c,e.

b) February 2016 case

From 12 to 14 February 2016, the TPV of interest in this case is transported into the middle latitudes, concurrent with a CAO over eastern North America. At 0000 UTC 12 February, the TPV is located over southern Hudson Bay and is moving southeastward downstream of the ridge over western North America (Fig. 8a). Like the January 1982 TPV, this TPV is collocated with a 1000–500-hPa thickness minimum (Fig 8b). However, in this case, the TPV and 1000–500-hPa cold pool are weaker in magnitude, characterized by minimum DT potential temperature and 1000–500-hPa thickness values of 270–273 K (Fig. 8a) and slightly below 480 dam (Fig. 8b), respectively at 0000 UTC 12 February. In addition, similar to the January 1982 case, there is a surface anticyclone located upstream of the TPV and associated cold pool (Fig. 8b). This anticyclone, however, only achieves a peak maximum MSLP of approximately 1046 hPa during its lifetime compared to 1062 hPa for the anticyclone in the January 1982 case. By 0000 UTC 13 February, the TPV, which has intensified slightly, has moved slowly southeastward along with the associated pool of arctic air and upstream anticyclone (Figs. 8c,d).

A pair of relatively small northerly flow jet streaks located downstream of the ridge at 0000 UTC 12 February (Fig. 8b) have consolidated into a single, more intense jet at 0000 UTC 13 February (Fig. 8d). By 0000 UTC 14 February, the TPV and associated cold pool have moved over New England, as the weakening surface anticyclone has moved over the Great Lakes (Figs. 8e–f). A surface ETC has strengthened and moved northeastward toward southeastern New England between 0000 UTC 13 and 14 February (Figs. 8d,f). This has resulted in an increased MSLP gradient downstream of the surface anticyclone. The nearly perpendicular orientation of the MSLP gradient to the 1000–500-hPa thickness gradient indicates relatively strong cold air advection occurring over and just offshore New England (Fig. 8f)

Figure 9 shows a meridional cross section transecting the TPV and associated pool of arctic air at 0000 UTC 14 February 2016. The TPV, indicated by PV values >2 PVU, extends downward to just below 600-hPa. Like the January 1982 TPV, isentropes bend upward beneath the TPV, indicative of the pool of arctic air found beneath the TPV. An upper-level front extends equatorward and downward from approximately 400 hPa near the TPV to approximately 800 hPa over the western North Atlantic beneath the polar jet. A strong meridional thermal gradient is evident south of the TPV over the western North Atlantic within the boundary layer where the cross-section transects the southern periphery of the pool of Arctic air. Beneath the TPV and over the western North Atlantic, a relatively deep, well-mixed boundary layer is noted, given the deep layer of $-\frac{\partial\theta}{\partial p} \leq 0$. This unstable air is likely resultant from the flow of arctic air over the relatively warm land and especially ocean surfaces. Similar to the January 1982 case, a shallow layer of relatively high PV air characterized by a large vertical potential temperature gradient extends poleward from TPV near the surface, indicative of the arctic air in place.

As investigated with the January 1982 case, the potential role of the TPV and associated pool of Arctic air in the strengthening of the upstream surface anticyclone is investigated for the February 2016 case. Figure 10 shows plots of Q_n and Q_s and their respective forcings for vertical motion from 1200 UTC 11 to 1200 UTC 12 February 2016, the time frame during which the surface anticyclone upstream of the TPV exhibits its greatest intensification rate of approximately 5 hPa in 24 hours, which is much smaller than the intensification rate exhibited by the January 1982 anticyclone (approximately 10 hPa in 12 hours). At 1200 UTC 11 February, a region of Q_n divergence and forcing for descent is noted just south of the 1042-hPa surface anticyclone over northern Canada, with Q_n vectors being directed toward warm air (Fig 10a). Q_s forcing is also located near and just southeast of the surface anticyclone, just upstream the trough axis extending westward from the TPV (Fig. 10b). However, the magnitude of Q_n and Q_s and their respective forcings for vertical motion in the vicinity of the location of the surface anticyclone are weaker in this case when compared to the magnitude of these quantities in January 1982 case. Like the January 1982 case, in the region of Q_n and Q_s forcing for descent, geostrophic cold air advection is evident in Figs. 10a,b, but is weaker in magnitude in this case as well (not shown). The presence of geostrophic cold air advection and Q_n vectors directed toward warm air indicated possible upper-level frontogenesis and a possible strengthening of the ageostrophic circulation in the entrance region of a 50 m s^{-1} northerly flow jet streak extending from northern Saskatchewan to the Great Lakes (not shown). The Q_n and Q_s forcing for descent suggest the surface anticyclone may strengthen slightly and move southeastward.

Indeed, by 0000 UTC 12 February, the surface anticyclone has moved southeastward and strengthened to 1046 hPa (Figs. 10c,d). Figures 10c,d indicate a slight increase and decrease of the forcing for descent by Q_n and Q_s respectively just southeast of the anticyclone. Geostrophic

cold air advection is still evident to the south of the surface anticyclone over northern Saskatchewan in the region of Q_n forcing for descent and implied frontogenesis given the orientation of the Q_n vectors from cold to warm air. The Q_n and Q_s forcings for descent southeast of the anticyclone lead to the southeastward movement and slight intensification of the anticyclone by 1200 UTC 12 February to 1047 hPa (Figs. 10e,f). The northerly flow jet streak has strengthened from 50 to 70 m s⁻¹ during the past 24 hours, possibly due to the previously mentioned forcing for upper-level frontogenesis. After 1200 UTC February, the surface anticyclone continues to move southeastward within the entrance region of the aforementioned jet streak, and weakens slowly (Figs. 8d,f).

6. Discussion and Conclusions

The impressive strengthening of the surface anticyclone in the January 1982 case coinciding with the interaction of the intense TPV with the strong upstream northerly flow jet, supports the hypothesis that TPV–jet interactions may lead the intensification of surface anticyclones in the jet left entrance region. This TPV–jet interaction leads to relatively strong Q_n forcing for descent in the jet left entrance region, contributing forcing for anticyclonogenesis. Furthermore, the TPV–jet interaction is associated with relatively strong forcing for upper-level frontogenesis, noted by the orientation of the Q_n vectors and the presence of geostrophic cold air advection. This forcing for upper-level frontogenesis potentially plays an important role in driving down the high PV, stratospheric air within the TPV downward toward 850-hPa, as evidenced in the cross section in Fig. 6. Compared to the January 1982 case, the Q_n and Q_s forcings for descent in the left entrance region of the northerly flow jet in the February 2016 case are weaker, and the rate of intensification of the surface anticyclone in this region is much

smaller. The February 2016 TPV is weaker, and further removed from the upper-level ridge and northerly flow jet at closest approach to these features compared to the January 1982 TPV (compare Fig. 8c to Fig 5c). With weaker TPV–jet interaction in the February 2016 case compared to the January 1982, there is less dynamical forcing for upper-level frontogenesis (weaker geostrophic cold air advection and weaker magnitude \mathbf{Q}_n vectors directed from cold to warm air) and simultaneously weaker forcing for descent near the location of the surface anticyclone in the jet entrance region (weaker \mathbf{Q}_n forcing for descent).

The potential strengthening of surface anticyclones due to TPV–jet interaction may lead to a stronger MSLP gradient downstream. In addition, because TPVs are associated with a surface-based pool of arctic air, the equatorward transport of TPVs may lead to a strengthening of the thermal gradient over the middle latitudes. The stronger MSLP and thermal gradients may contribute to strong lower-tropospheric cold air advection, as occurred especially in the January 1982 case. In addition, regardless of the strength of cold air advection, because TPVs appear to be collocated with surface-based pools of arctic air, locations beneath and nearby TPV may experience bitterly cold arctic air, evident in both the January 1982 and February 2016 cases.

In both cases, ETCs over the North Pacific appear to play important roles in the downstream ridge development and amplification crucial to the extraction of the TPVs over North America and subsequent CAO development. Predictability of these ETCs may impact the downstream predictability of TPV extraction and CAO development. Therefore, improved forecasting of upstream precursor disturbances responsible for ridge amplification and subsequent downstream transport of TPVs to middle latitudes may lead to improved forecasts of CAOs occurring in the middle latitudes.

REFERENCES

- Bosart, L. F., G. J. Hakim, K. R. Tyle, M. A. Bedrick, W. E. Bracken, M. J. Dickinson, and D. M. Schultz, 1996: Large-scale antecedent conditions associated with the 12–14 March 1993 cyclone (“superstorm ‘93”) over eastern North America. *Mon. Wea. Rev.*, **124**, 1865–1891.
- Cavallo, S. M., and G. J. Hakim, 2009: Potential vorticity diagnosis of a tropopause polar cyclone. *Mon. Wea. Rev.*, **137**, 1358–1371.
- Cavallo, S. M., and G. J. Hakim, 2010: The composite structure of tropopause polar cyclones from a mesoscale model. *Mon. Wea. Rev.*, **138**, 3840–3857.
- Colucci, S. J., and J. C. Davenport, 1987: Rapid surface anticyclogenesis: Synoptic climatology and attendant large scale circulation changes. *Mon. Wea. Rev.*, **115**, 822–836.
- Emanuel, K., 2008: Back to Norway: An Essay. *Meteorological Monographs*, **33**, 87–96.
- Hakim, G. J., L. F. Bosart, and D. Keyser, 1995: The Ohio Valley wave-merger cyclogenesis event of 25–26 January 1978. Part I: Multiscale case study. *Mon. Wea. Rev.*, **123**, 2663–2692.
- Hakim, G. J., D. Keyser, and L. F. Bosart, 1996: The Ohio Valley wave-merger cyclogenesis event of 25–26 January 1978. Part II: Diagnosis using quasigeostrophic potential vorticity inversion. *Mon. Wea. Rev.*, **124**, 2176–2205.
- Hakim, G. J. and A. K. Canavan, 2005: Observed cyclone-anticyclone tropopause asymmetries. *J. Atmos. Sci.*, **62**, 231–240.
- Hoskins, B. J., and M. A. Pedder, 1980: The diagnosis of middle latitude synoptic development. *Quart. J. Roy. Meteor. Soc.*, **106**, 707–719.
- Hoskins, B. J., M. E. McIntyre, and A. W. Robertson, 1985: On the use and significance of

- isentropic potential vorticity maps. *Quart. J. Roy. Meteor. Soc.*, **111**, 877–956.
- Jones, J.E. and J. Cohen, 2011: A diagnostic comparison of Alaskan and Siberian strong anticyclones. *J. Climate*, **24**, 2599–2611.
- Keyser, D., B. D. Schmidt, and D. G. Duffy, 1992: Quasigeostrophic vertical motions diagnosed from along- and crossisentrope components of the Q vector. *Mon. Wea. Rev.*, **120**, 731–741.
- Kravitz, J. R., 2007: A study of coherent tropopause disturbances from a climatological perspective. M.S. thesis, Department of Earth and Atmospheric Sciences, University at Albany/SUNY, Albany, NY, 191 pp.
- Pyle, M. E., D. Keyser, and L. F. Bosart, 2004: A diagnostic study of jet streaks: Kinematic signatures and relationship to coherent tropopause disturbances. *Mon. Wea. Rev.*, **132**, 297–319.
- Saha, S., and Coauthors, 2010: The NCEP climate forecast system reanalysis. *Bull. Amer. Meteor. Soc.*, **91**, 1015–1057. 27
- Saha, S., and Coauthors, 2014: The NCEP climate forecast system version 2. *J. Climate*, **27**, 2185–2208.
- Shapiro, M. A., 1981: Frontogenesis and geostrophically forced secondary circulations in the vicinity of jet stream-frontal zone systems. *J. Atmos. Sci.*, **38**, 954–973.
- Shapiro, M. A., T. Hampel and A. J. Krueger, 1987: The Arctic tropopause fold. *Mon. Wea. Rev.*, **115**, 444–454.
- Thorpe, A. J., 1985: Diagnosis of balanced vortex structure using potential vorticity. *J. Atmos. Sci.*, **42**, 397–406.

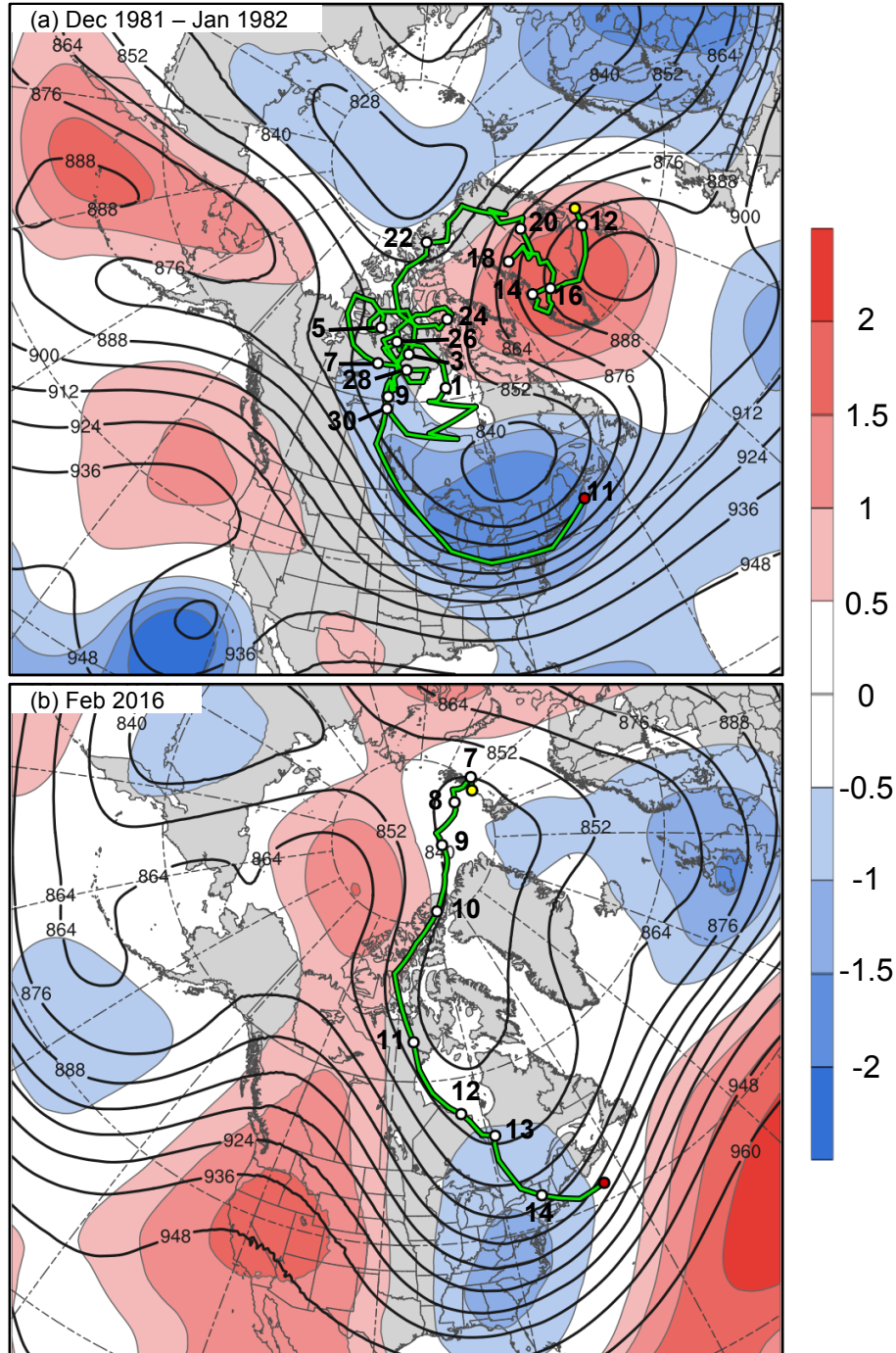


FIG. 2. Time mean 300-hPa geopotential height (contoured in black every 12 dam) and standardized anomaly of geopotential height (σ , shaded) for (a) 7 January – 11 January 1982 and (b) 6 – 14 February 2016. Green line denotes TPV track for (a) 1800 UTC 11 December 1981 – 0000 UTC 11 January 1982 and (b) 1800 UTC 6 February – 1800 UTC 14 February 2016. White dots denote 0000 UTC times along TPV track every (a) 48 hours and (b) 24 hours. Each white dot is labeled with a number denoting the date. Yellow and red dots denote the beginning and end points, respectively, of each TPV track.

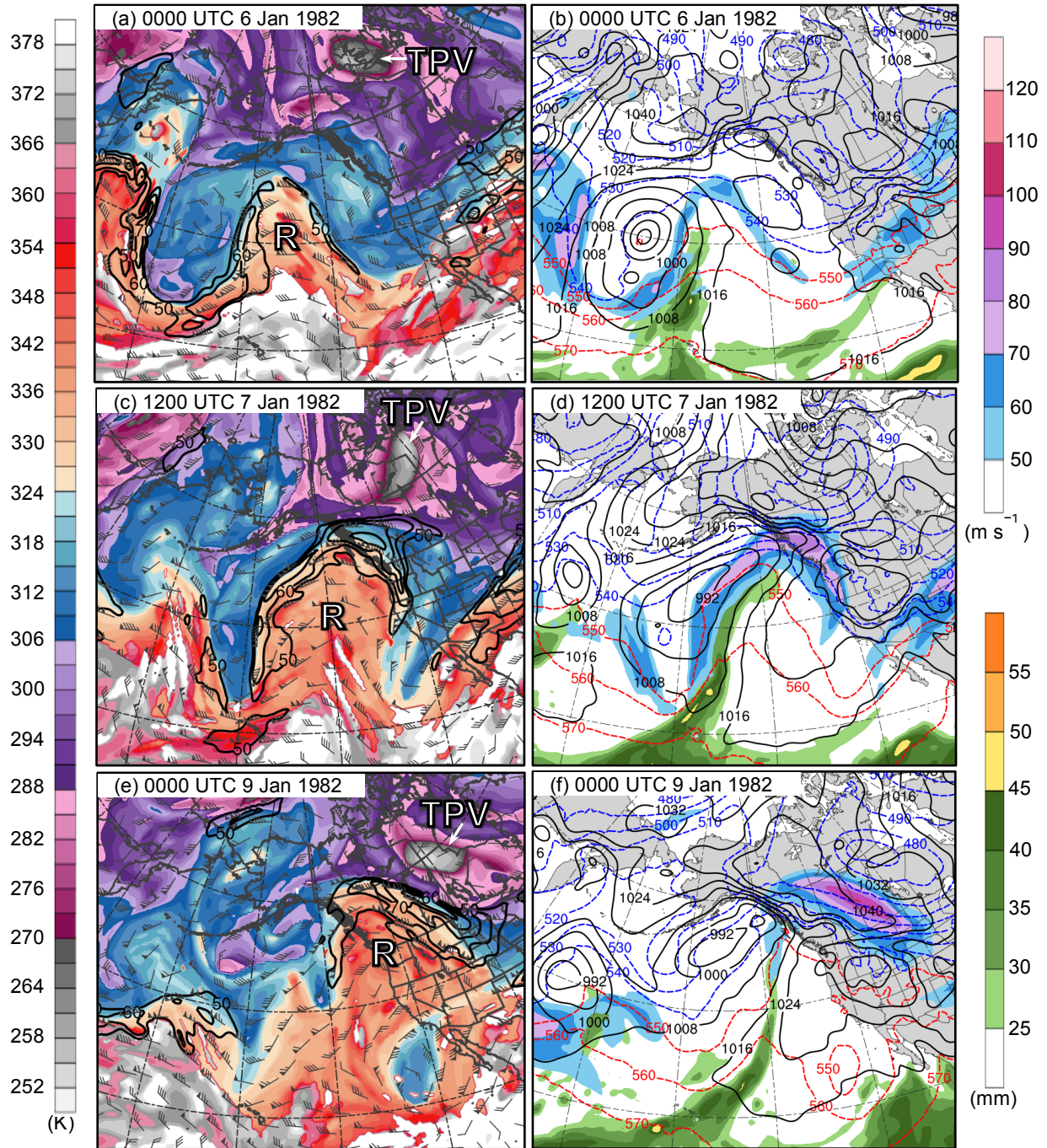


FIG. 3. Analysis of DT (2-PVU surface) potential temperature (shaded, K), wind speed (black contours every 10 m s^{-1} , beginning at 50 m s^{-1}), and wind (flags and barbs, m s^{-1}) at (a) 0000 UTC 6 January, (c) 1200 UTC 7 January, and (e) 0000 UTC 9 January; 250-hPa wind speed (shaded, m s^{-1}), 1000–500-hPa thickness (dashed red and blue contours every 10 dam, contoured red for greater than 540 dam and blue otherwise), mean sea-level pressure (MSLP, black contours every 8 hPa), and precipitable water (shaded, mm) at (b) 0000 UTC 6 January, (d) 1200 UTC 7 January, and (f) 0000 UTC 9 January 1982. Labels “TPV” and “R” represent location of the TPV and ridge of interest, respectively.

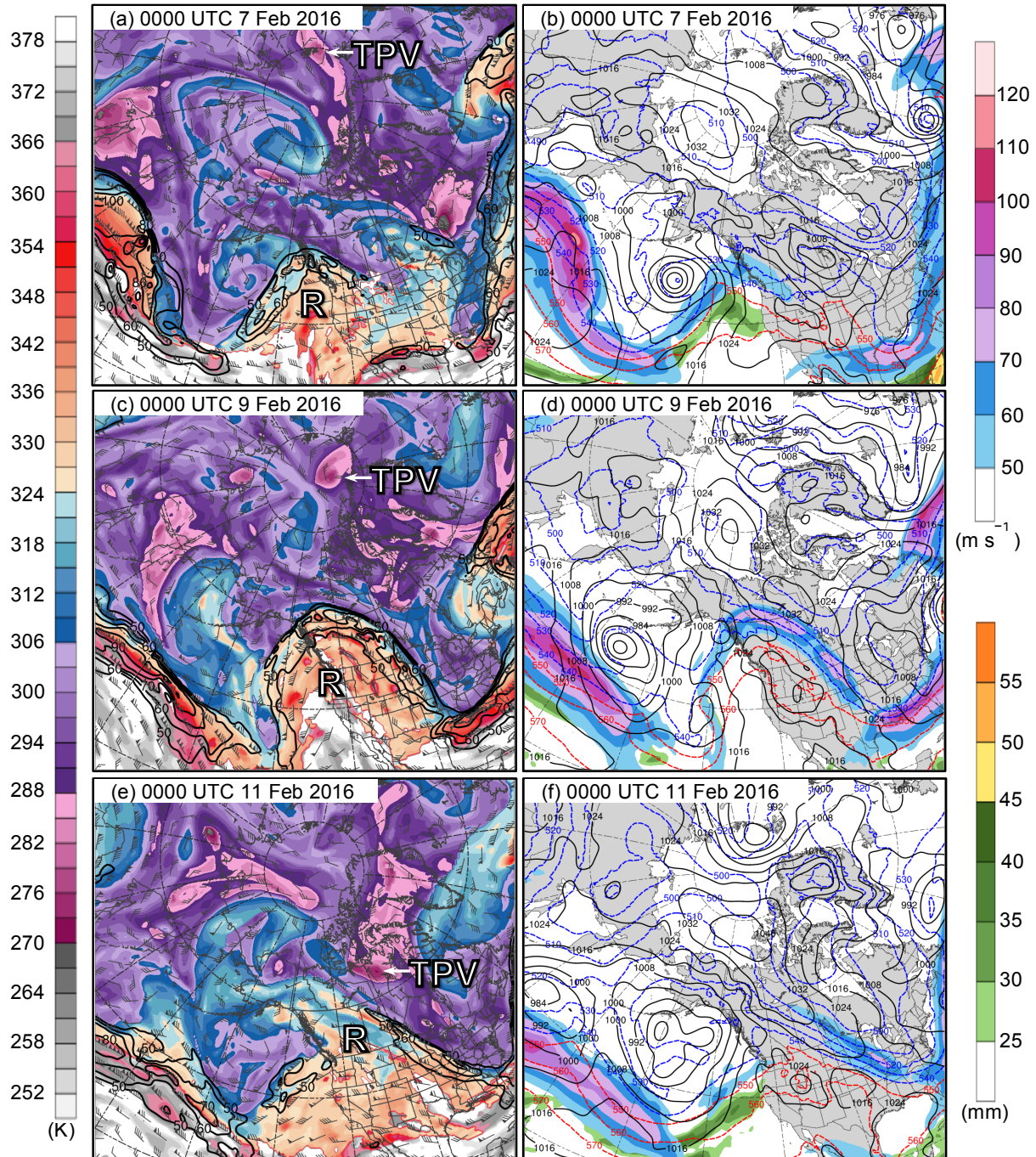


FIG. 4. Analysis of DT (2-PVU surface) potential temperature (shaded, K), wind speed (black contours every 10 m s^{-1} , beginning at 50 m s^{-1}), and wind (flags and barbs, m s^{-1}) at (a) 0000 UTC 7 February, (c) 0000 UTC 9 February, and (e) 0000 UTC 11 February; 250-hPa wind speed (shaded, m s^{-1}), 1000–500-hPa thickness (dashed red and blue contours every 10 dam, contoured red for greater than 540 dam and blue otherwise), mean sea-level pressure (MSLP, black contours every 8 hPa), and precipitable water (shaded, mm) at (b) 0000 UTC 7 February, (d) 0000 UTC 9 February, and (f) 0000 UTC 11 February 2016. Labels “TPV” and “R” represent location of the TPV and ridge of interest, respectively.

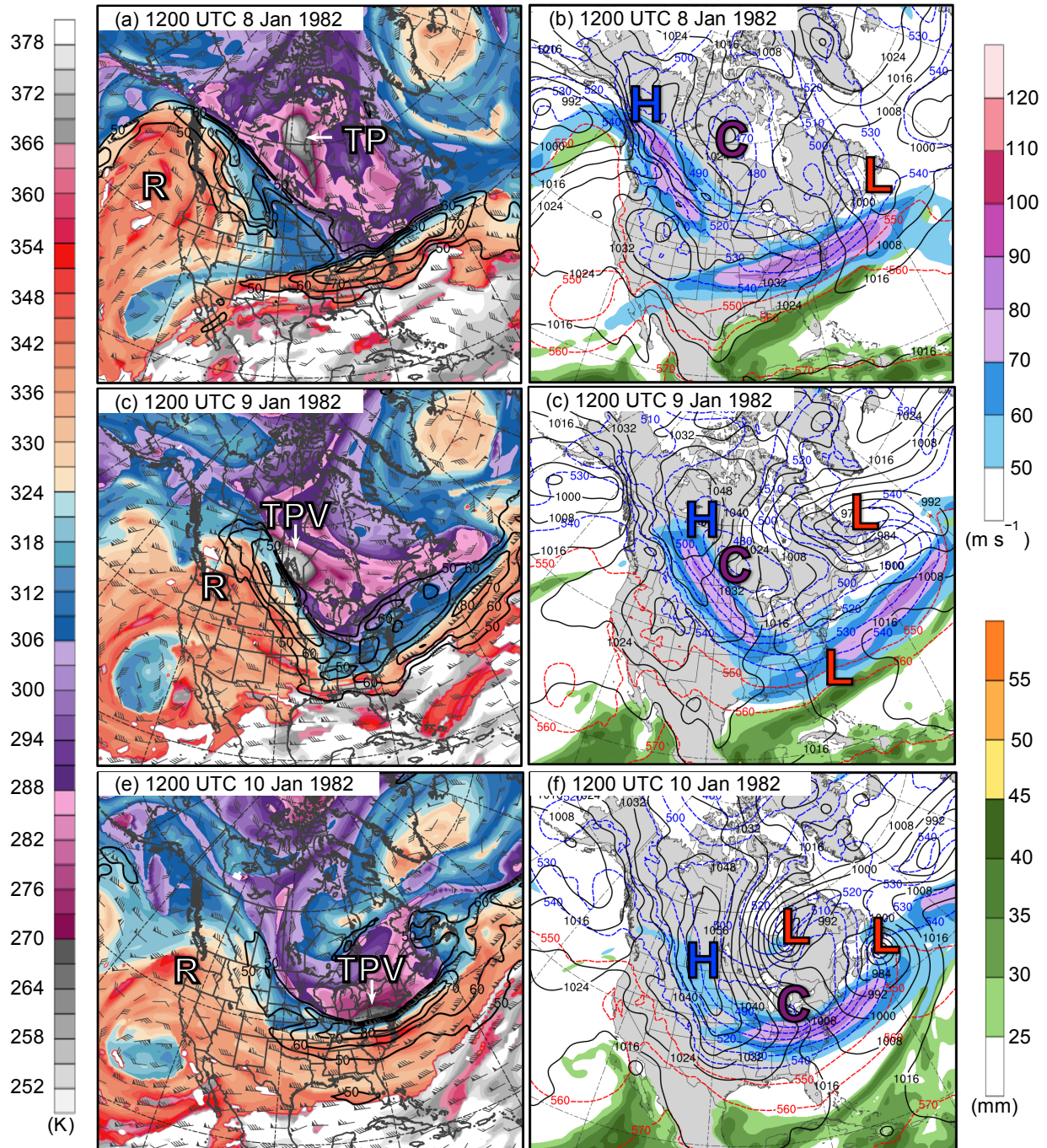


FIG. 5. Analysis of DT (2-PVU surface) potential temperature (shaded, K), wind speed (black contours every 10 m s^{-1} , beginning at 50 m s^{-1}), and wind (flags and barbs, m s^{-1}) at (a) 1200 UTC 8 January, (c) 1200 UTC 9 January, and (e) 1200 UTC 10 January; 250-hPa wind speed (shaded, m s^{-1}), 1000–500-hPa thickness (dashed red and blue contours every 10 dam, contoured red for greater than 540 dam and blue otherwise), mean sea-level pressure (MSLP, black contours every 8 hPa), and precipitable water (shaded, mm) at (b) 1200 UTC 8 January, (d) 1200 UTC 9 January, and (f) 1200 UTC 10 January 1982. Labels “TPV,” “R,” “C,” “H,” and “L” represent location of the TPV, ridge, cold pool, surface anticyclone, and surface cyclones of interest, respectively.

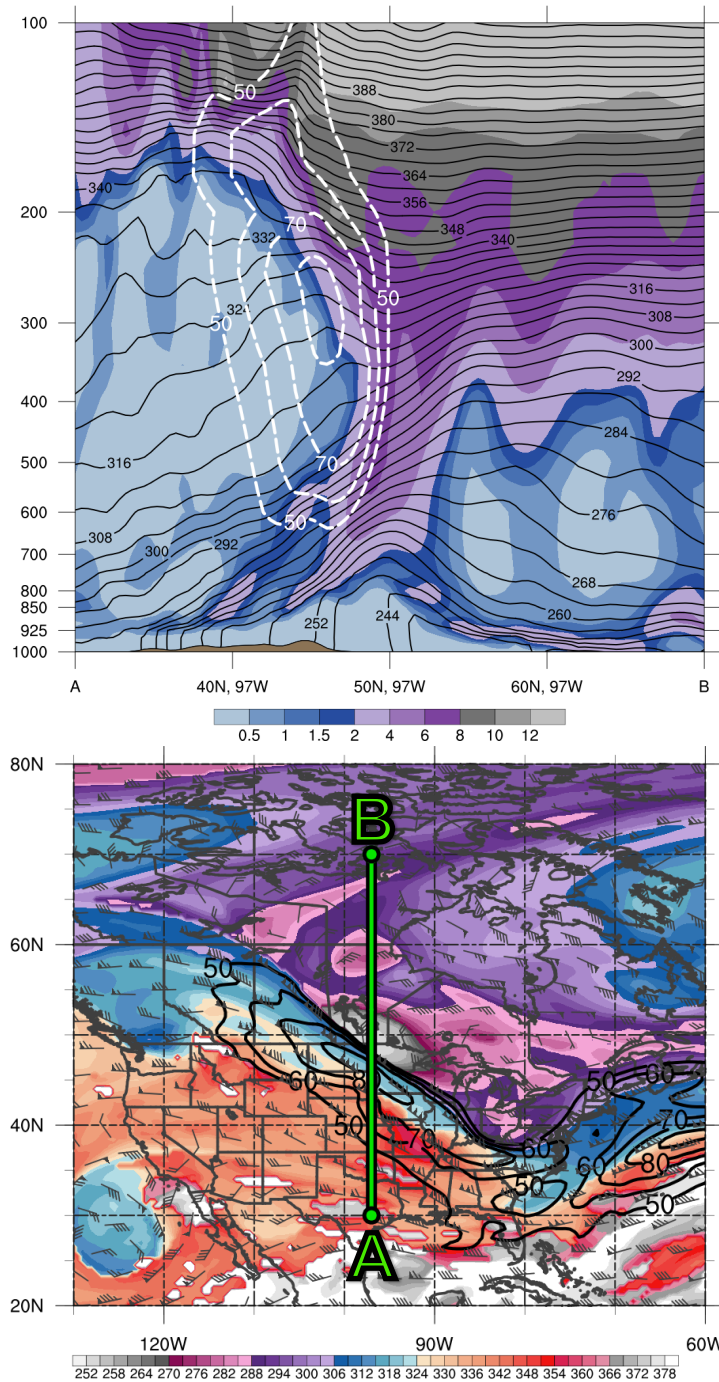


FIG. 6. (top) Cross section along line AB of PV (PVU, shaded), potential temperature (K, black), and wind speed (m s^{-1} , dashed white contours), and (bottom) DT (2-PVU surface) potential temperature (shaded, K), wind speed (black contours every 10 m s^{-1} , beginning at 50 m s^{-1}), and wind (flags and barbs, m s^{-1}) at 1800 UTC 9 January 1982. Green line in bottom panel represents transect of cross section AB.

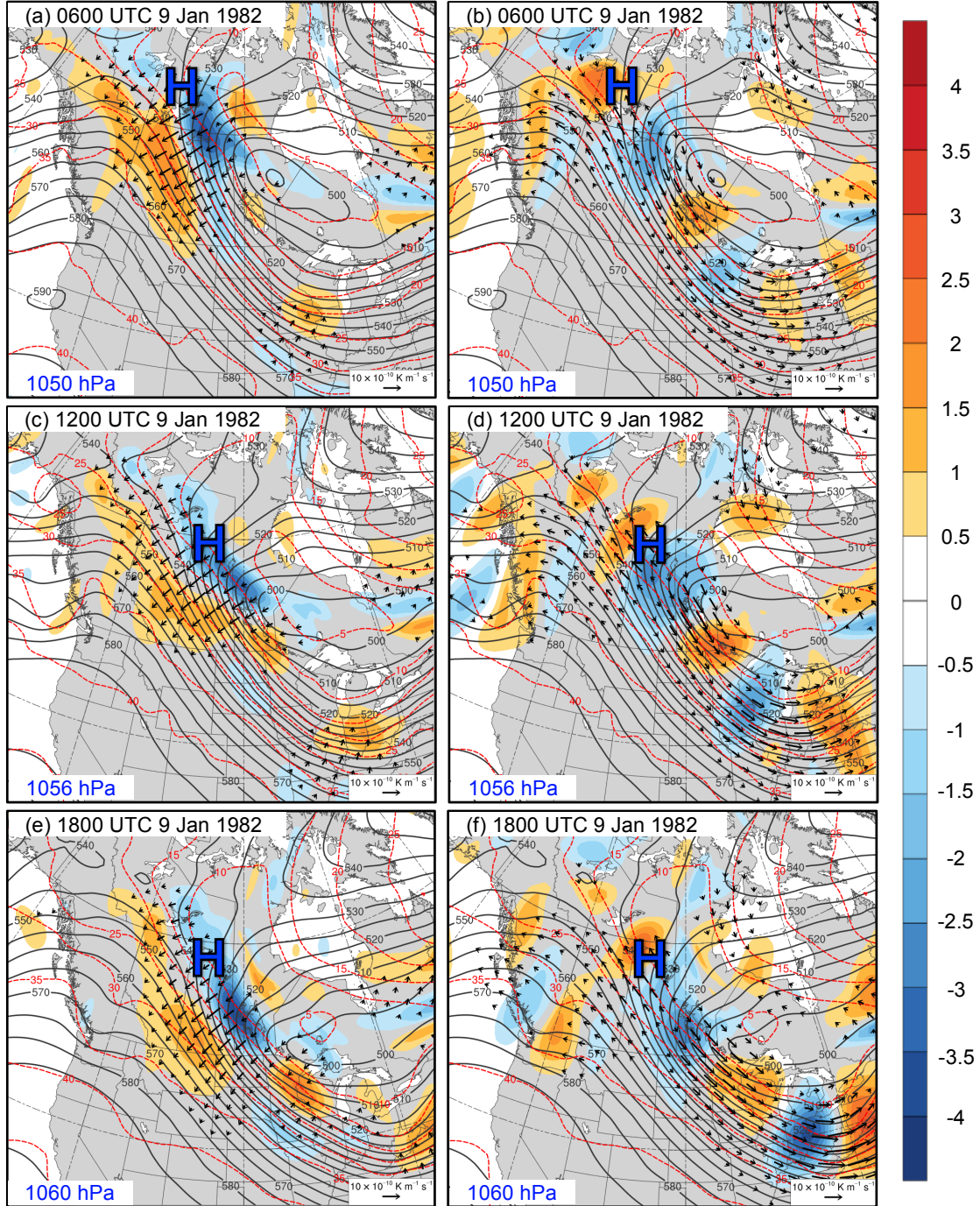


FIG. 7. 600–400-hPa Q_n ($K m^{-1} s^{-1}$, vectors), Q_n forcing for vertical motion ($\times 10^{-18} Pa^{-1} s^{-3}$, shaded), geopotential height (dam, gray), and potential temperature (K, red) at (a) 0600 UTC 9 January, (c) 1200 UTC 9 January, and (e) 1800 UTC 9 January; 600–400-hPa Q_s ($K m^{-1} s^{-1}$, vectors), Q_s forcing for vertical motion ($\times 10^{-18} Pa^{-1} s^{-3}$, shaded), geopotential height (dam, gray), and potential temperature (K, red) at (b) 0600 UTC 9 January, (d) 1200 UTC 9 January, and (f) 1800 UTC 9 January 1982. Label “H” represents location of maximum MSLP of surface anticyclone of interest at each time. Maximum MSLP (in hPa) of surface anticyclone of interest at each time is given in bottom-left corner of each panel.

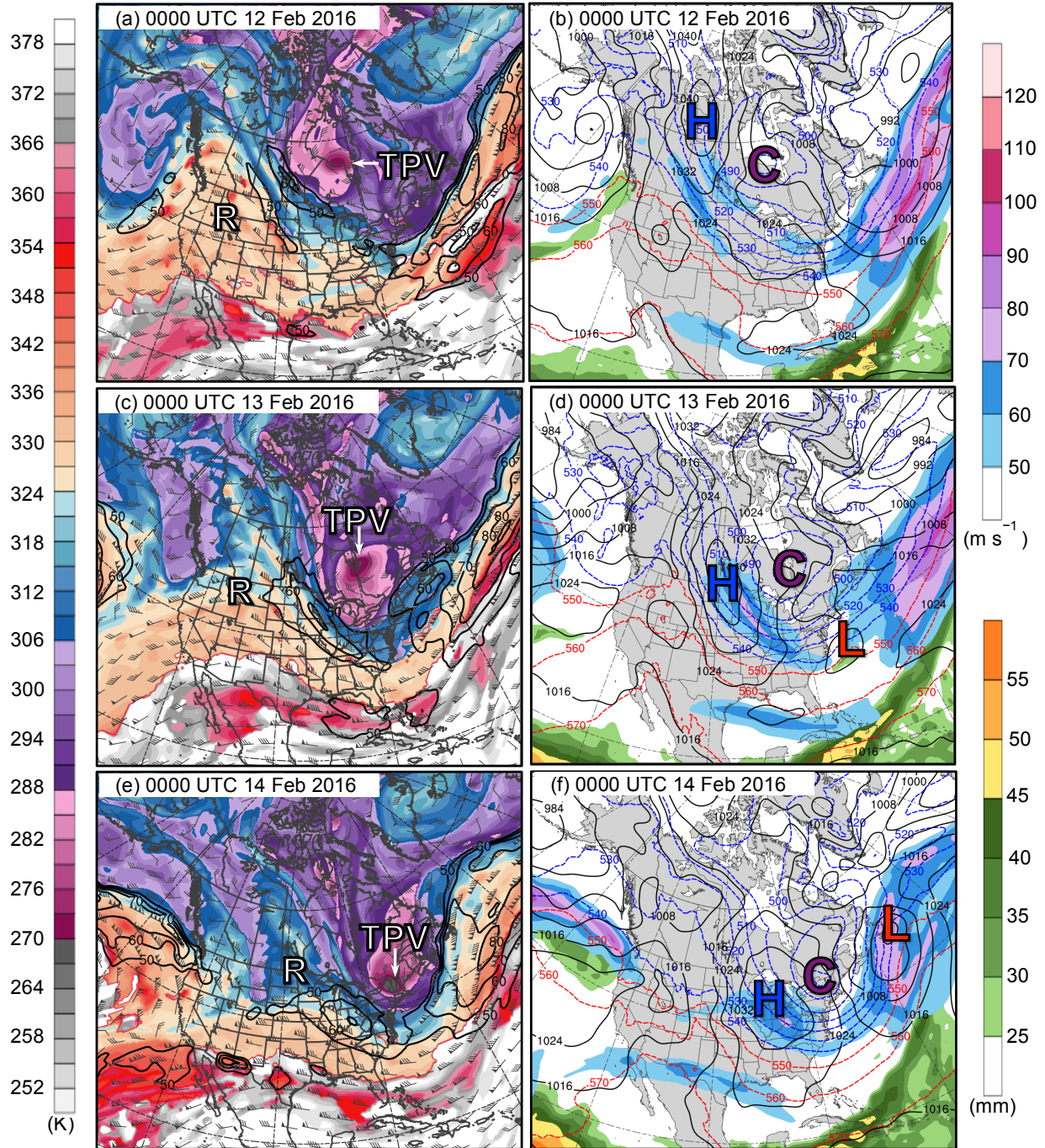


FIG. 8. Analysis of DT (2-PVU surface) potential temperature (shaded, K), wind speed (black contours every 10 m s^{-1} , beginning at 50 m s^{-1}), and wind (flags and barbs, m s^{-1}) at (a) 0000 UTC 12 February, (c) 0000 UTC 13 February, and (e) 0000 UTC 14 February; 250-hPa wind speed (shaded, m s^{-1}), 1000–500-hPa thickness (dashed red and blue contours every 10 dam, contoured red for greater than 540 dam and blue otherwise), mean sea-level pressure (MSLP, black contours every 8 hPa), and precipitable water (shaded, mm) at (b) 0000 UTC 12 February, (d) 0000 UTC 13 February, and (f) 0000 UTC 14 February 2016. Labels “TPV,” “R,” “C,” “H,” and “L” represent location of the TPV, ridge, cold pool, surface anticyclone, and surface cyclones of interest, respectively.

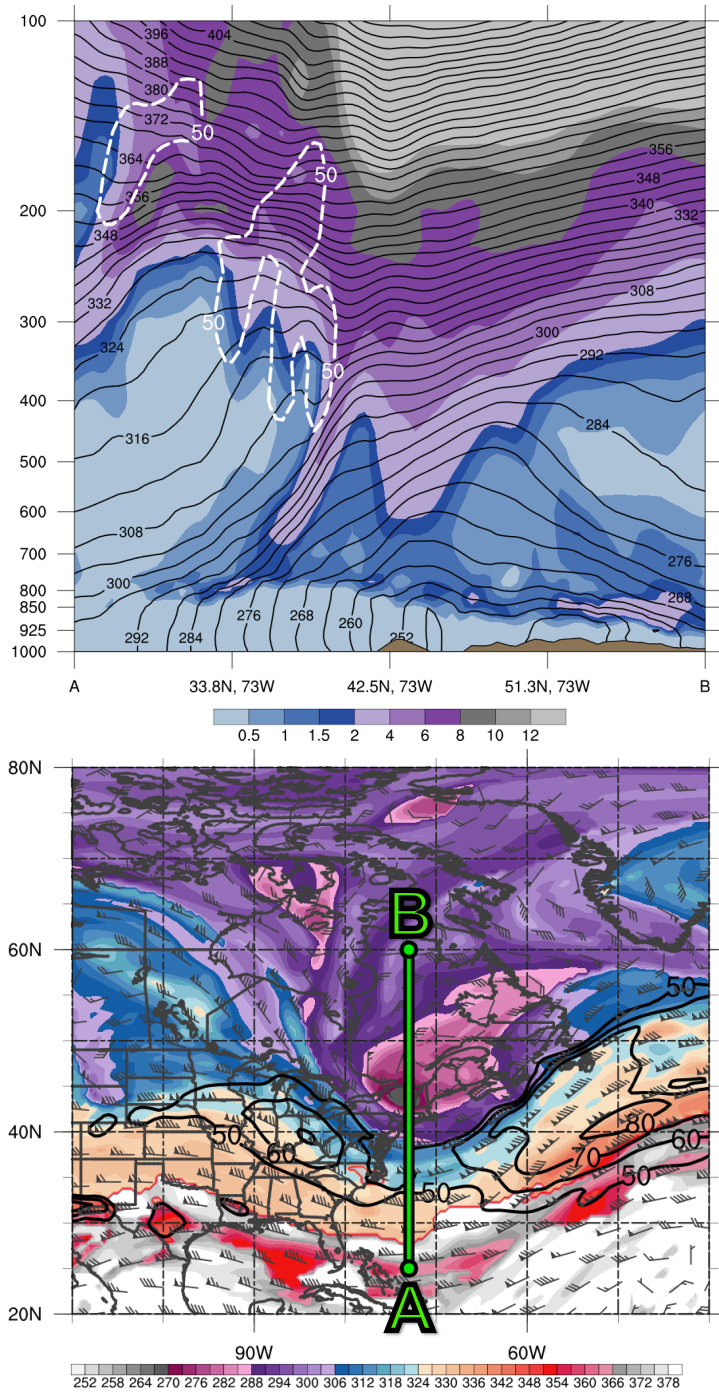


FIG. 9. (top) Cross section along line AB of PV (PVU, shaded), potential temperature (K, black), and wind speed (m s^{-1} , dashed white contours), and (bottom) DT (2-PVU surface) potential temperature (shaded, K), wind speed (black contours every 10 m s^{-1} , beginning at 50 m s^{-1}), and wind (flags and barbs, m s^{-1}) at 0000 UTC 14 February 2016. Green line in bottom panel represents transect of cross section AB.

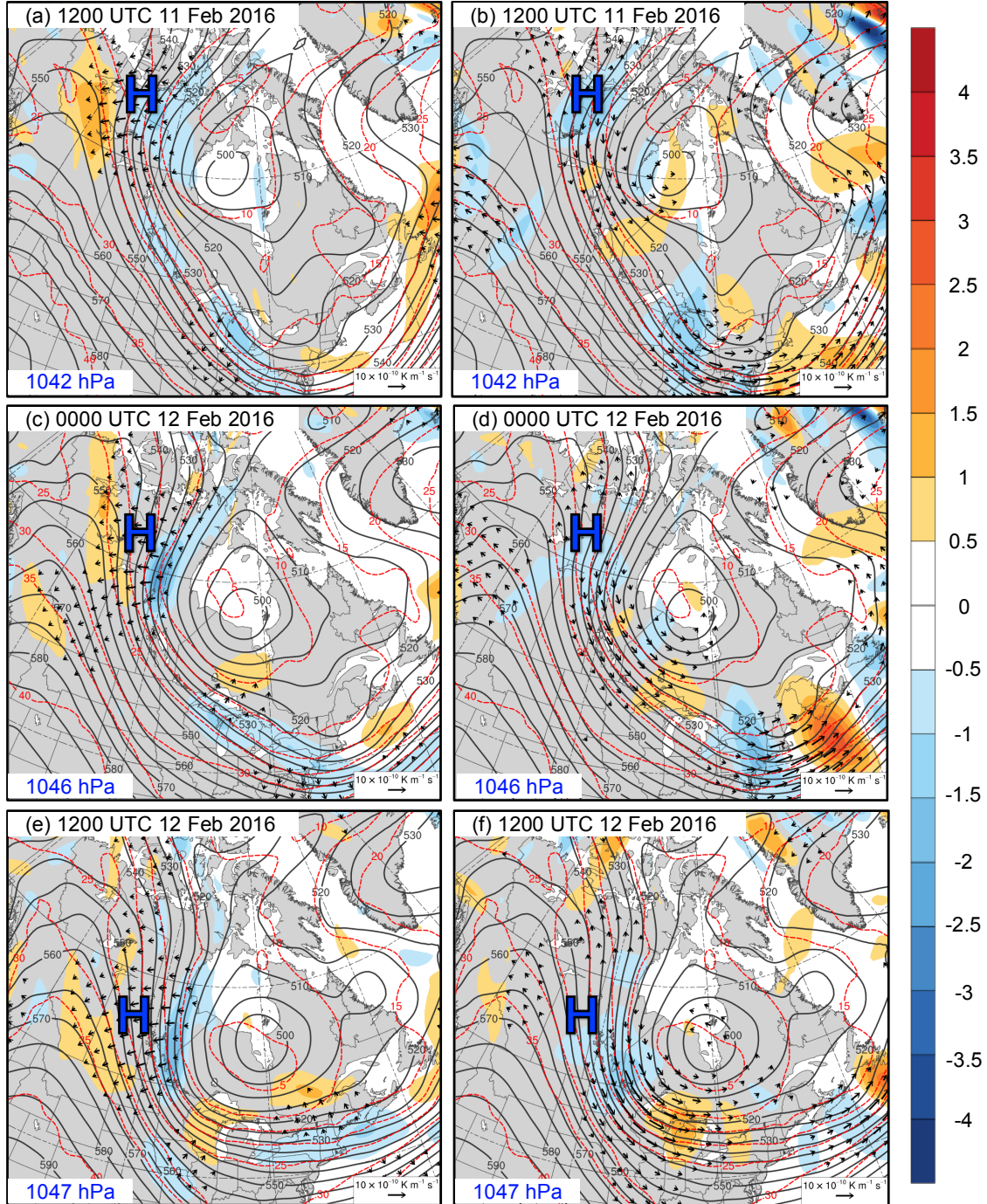


FIG. 10. 600–400-hPa Q_n ($K m^{-1} s^{-1}$, vectors), Q_n forcing for vertical motion ($\times 10^{-18} Pa^{-1} s^{-3}$, shaded), geopotential height (dam, gray), and potential temperature (K, red) at (a) 1200 UTC 11 February, (c) 0000 UTC 12 February, and (e) 1200 UTC 12 February; 600–400-hPa Q_s ($K m^{-1} s^{-1}$, vectors), Q_s forcing for vertical motion ($\times 10^{-18} Pa^{-1} s^{-3}$, shaded), geopotential height (dam, gray), and potential temperature (K, red) at (b) 1200 UTC 11 February, (d) 0000 UTC 12 February, and (f) 1200 UTC 12 February 2016. Label “H” represents location of maximum MSLP of surface anticyclone of interest at each time. Maximum MSLP (in hPa) of surface anticyclone of interest at each time is given in bottom-left corner of each panel.